Supporting Information

In Vivo High-resolution Ratiometric Fluorescence Imaging of Inflammation Using NIR-II Nanoprobes with 1550 nm Emission

*Shangfeng Wang[1], Lu Liu[1], Yong Fan[1], Ahmed Mohamed El-Toni[2], Mansour Saleh Alhoshan[3], Dandan li[1] and Fan Zhang[1]**

[1]Department of Chemistry, State Key Laboratory of Molecular Engineering of Polymers, Shanghai Key Laboratory of Molecular Catalysis and Innovative Materials and iChem, Fudan University, Shanghai 200433, P. R. China

[2]King Abdullah Institute for Nanotechnology, King Saud University, Riyadh 11451, Saudi Arabia

[3]Department of Chemical Engineering, King Saud University, Riyadh 11421, Saudi Arabia

[*]*Correspondence should be addressed to F.Z. (zhang_fan@fudan.edu.cn)*

Experimental section

Chemicals

Erbium (III) acetate hydrate (99.9%), yttrium (III) acetate hydrate (99.9%), yttrium (III) chloride hexahydrate (99.9%), ytterbium acetate hydrate (99.9%), sodium trifluoroacetate (Na-TFA, 98 %), 1-octadecene (ODE, 90%), oleic acid (OA, 90%) were purchased from Sigma-Aldrich. 1,2-distearoyl-sn-glycero-3-phosphoethanolamine-N-[methoxy(polyethylene glycol)-2000] (DSPE-mPEG), 1,2-distearoyl-sn-glycero-3-phosphoethanolamine-N-[dibenzocyclooctyne-(polyethylene glycol)-2000] (DSPE-PEG-DBCO) and 1,2-distearoyl-sn-glycero-3-phosphoethanolamine-N-[azide-(polyethylene glycol)-2000] (DSPE-PEG-N_3) were purchased from Avanti Polar Lipids. Analytical grade solvents including NaOH, NH_4F, petroleum Ether, CH_2Cl_2, and EtOAc were purchased from Titan Scientific. All other chemicals were purchased from TCI and J&K without further purification unless otherwise noted.

Preparation of shell precursors

Y-OA (0.10 M) host precursor: a mixture of YCl_3 (5 mmol), OA (20.0 mL), and ODE (30.0 mL) was loaded in a reaction container and heated at 140 °C under vacuum with magnetic stirring for 30 min to remove residual water and oxygen. Then the colorless Y-OA precursor solution (0.10 M) was obtained.

Na-TFA-OA (0.40 M) precursor: A mixture of Na-TFA (4.00 mmol) and OA (10.0 mL) was loaded in a container at room temperature under vacuum with magnetic stirring to remove residual water and oxygen. Then the colorless Na-TFA-OA precursor solution (0.40 M) was obtained.

Synthesis of β-$NaY_xEr_{1-x}F_4$ core nanoparticles

Hexagonal phase (β) $NaY_xEr_{1-x}F_4$ (X mol% Y^{3+}) doped nanocrystals were synthesized following a previously reported thermolysis method.[1] Calculated amounts of $Er(CH_3CO_2)_3 \cdot 4H_2O$, $Y(CH_3CO_2)_3 \cdot 4H_2O$ to a total of 1.0 mmol, In a typical synthesis, OA (6.0 mL) and ODE (15.0 mL) were mixed together and heated to 140 °C under vacuum until a clear solution formed, after that, the solution was cooled down to room temperature. To this solution at room temperature, a methanol solution (10.0 mL) of ammonium fluoride (4 mmol) and sodium hydroxide (2.5 mmol) was added and stirred for 1 h. The reaction mixture was then heated to 70 °C and maintained for half an hour to remove the methanol. Afterward, the solution was heated to 300 °C (~10 °C/min) and maintained for 60 min under a gentle argon flow. Then, the solution was cool down to room temperature and the nanoparticle products were centrifuged and washed twice with ethanol. The nanoparticles were finally dispersed in 10 mL of cyclohexane for further use.

Synthesis of β-$NaY_xEr_{1-x}F_4$@$NaYF_4$ core-shell nanoparticles

The core-shell nanoparticles were fabricated by using the one-pot successive layer-by-layer (SLBL) protocol, which was developed by our group.[2] 2.5 mL of the purified $NaY_xEr_{1-x}F_4$ core nanoparticles solution (~ 0.25 mmol) were mixed with 4.0 mL of OA and 6.0 mL of ODE. The flask was pumped down at 70 °C for 30 min to remove cyclohexane, along with any residual air. Subsequently, the system was switched to Ar flow and the reaction mixture was further heated to 280 °C at a rate of ~20 °C/min. Then pairs of Y-OA (0.10 M, 1.0 mL) and Na-TFA-OA (0.40 M, 0.50 mL) precursors were alternately introduced by dropwise addition at 280 °C and the time interval between each injection was 15 min. The shell thickness can be well tuned by changing the addition times or the amount (no more than 2.5 mmol Re-OA precursor each time) of the shell precursors. Finally, the obtained $NaY_xEr_{1-x}F_4$@$NaYF_4$ core/shell nanoparticles were precipitated and washed in the same way as the core nanoparticles were and dispersed in cyclohexane.

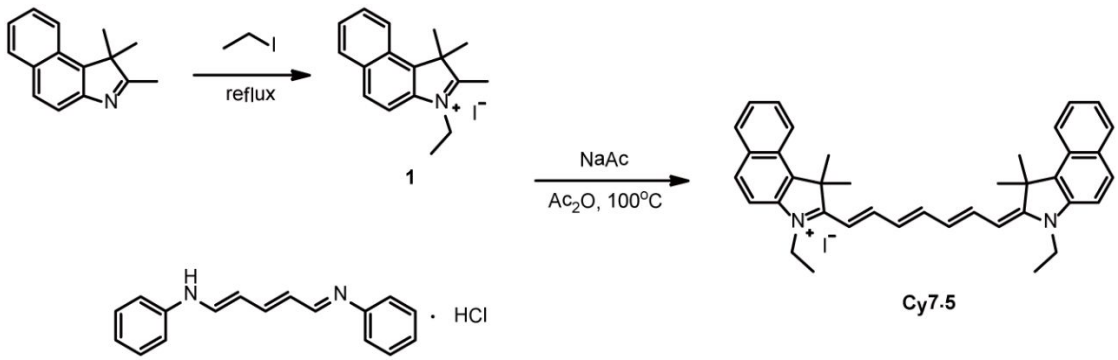

Scheme S1. Synthetic procedure of Cy7.5.

Synthesis of compound 1

1,1,2-Trimethyl-1H-benz[e]indole (1.05 g, 5 mmol) was dissolved in 5 mL ethyl iodide and refluxed at 80 °C overnight. The reaction solution was cooled to room temperature and ether was used to precipitate the product from solution to yield 1.5 g (82%) of compound **1**.

Synthesis of Cy7.5

To a mixture of N-[5-(phenylamino)-2,4-pentadienylidene]aniline monohydrochloride (284.78 mg, 1 mmol), NaOAc (82 mg, 1 mmol) and Compound **1** (730.5 mg, 2 mmol) was added Ac_2O (8 mL) and subsequently heated at 100 °C under nitrogen for 2 h. After cooling to room temperature, ether was poured into the solution and the precipitate was purified by a flash column chromatography [silica gel, MeOH/DCM = 0/50 to 1/50, v/v] to give **Cy7.5** (yield: 800 mg,

60%). ^{1}H NMR (400 MHz, $CDCl_3$) δ 8.12 (d, J = 8.6 Hz, 2H), 7.94 (t, J = 16.2 Hz, 7H), 7.59 (t, J = 7.6 Hz, 2H), 7.44 (t, J = 7.5 Hz, 2H), 7.35 (d, J = 8.8 Hz, 2H), 6.69 (s, 2H), 6.28 (d, J = 12.1 Hz, 2H), 4.23 (d, J = 6.4 Hz, 4H), 1.99 (s, 12H), 1.48 (t, J = 7.1 Hz, 6H); Maldi-Tof/Tof-MS: calcd for $C_{39}H_{41}N_2^+$ $[M]^+$, 537.3264; Found, 537.2692. $[M]^+$.

Preparation of NIR-II biosensing nanoprobe DCNP@Cy7.5

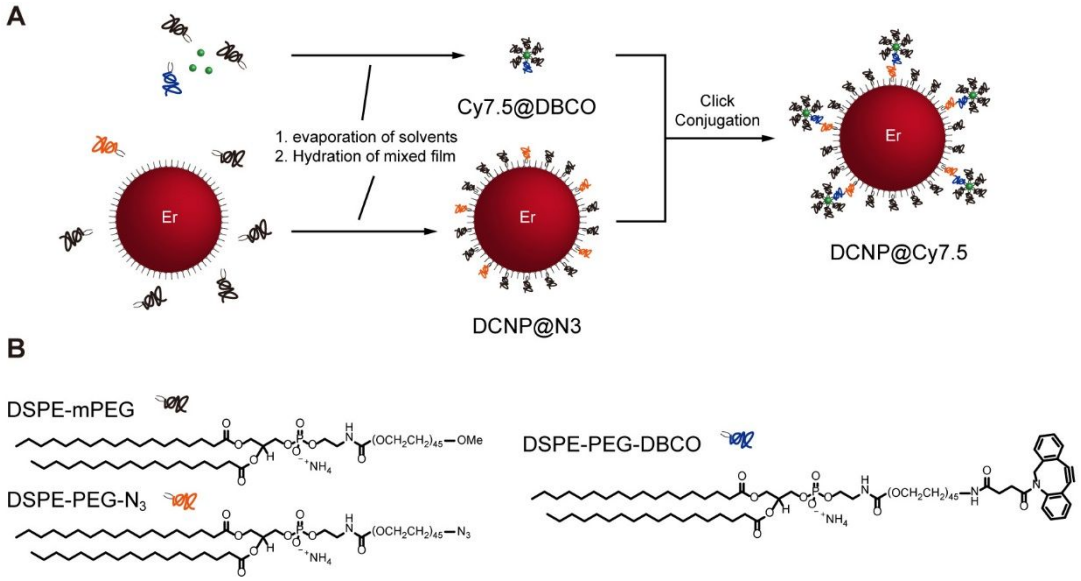

Scheme S2. (A) Schematic representation of the preparation of Cy7.5@DBCO, DCNP@N_3 and DCNP@Cy7.5. (B) Molecular structures of PEGylated phospholipids with different fuctional groups.

Preparation of Cy7.5-loaded nanomicelles (Cy7.5@DBCO)

Cy7.5 were firstly dissolved in $CHCl_3$ to obtain stock solution with concentration of 5 mM. 100 μL stock solution of Cy7.5 was mixed with 640 μL DSPE-PEG (25 mg/mL in $CHCl_3$, DSPE-mPEG:DSPE-PEG-DBCO (*mol*/*mol*) = 9:1) at a mass ratio of ~2:100. The solvent was removed by vacuum rotary evaporation to form a dry dye-containing lipid film. The dried film was hydrated with 10 mL deionized water at 80 °C and sonication for 1 minute to obtain the Cy7.5@DBCO with final Cy7.5 concentration of 50 μM.

Preparation of phospholipids-capped DCNP (DCNP@N_3)

All the DCNPs with different Er^{3+}-doped concentration were used the same method as follows: the oleic acid capped DCNPs (0.1 mmol for Ln^{3+} in core) in 5 mL of chloroform was mixed with 5 mL DSPE-PEG (25 mg/mL in $CHCl_3$, DSPE-mPEG:DSPE-PEG-N_3 (*mol*/*mol*) = 9:1). The solvent was removed by vacuum rotary evaporation to form a dry dye-containing lipid film. The dried film was hydrated with 10 mL deionized water at 80 °C and sonication for 5 minutes

to obtain a clear solution. Excess lipids were purified from the solution by ultracentrifugation (100000 rpm, 10 min) and washing (3X). The solution was further concentrated to obtain the final DCNP@N_3 stock solution with a concentration of ~13.55 mg/mL (nanocrystal) according to the ICP-AES results.

Preparation of DCNP@Cy7.5

200 μL of DCNP@N_3 was mixed with varying volumes of Cy7.5@DBCO (50 μM) and allowing to stir at room temperature overnight. After ultracentrifugation at 100000 rpm for 10 min, completed click conjugation were confirmed by the zero absorption of Cy7.5 in supernatants for all groups. Therefore, the as-prepared DCNP@Cy7.5 were diluted to 1 mL with deionized water and used for the next experiments without further purification. The concentration of nanocrystal in DCNP@Cy7.5 was measured to be ~2.4 mg/mL containing ~0.26 mg/mL of Er^{3+} (ICP-AES).

Characterization

Transmission electron microscopy (TEM), high-resolution transmission electron microscopy (HRTEM), observations were performed with a JEM-2100F transmission electron microscope with an accelerating voltage of 200 kV equipped with a post column Gatan imaging filter (GIF-Tri-dium). ^{1}H-NMR and ^{13}C-NMR spectra were acquired on a Bruker AV-400 spectrometer. Chemicals shifts are referenced to the residue solvent peaks and given in ppm. MALDI-TOF MS analyses were performed in positive reflection mode on a 5800 proteomic analyzer (Applied Biosystems, Framingham, MA, USA) with a Nd:YAG laser at 355 nm, a repeti-tion rate of 400 Hz, and an acceleration voltage of 20 kV. Dynamic light scattering (DLS) were carried out on a Malvern Zetasizer 3600 (Malvern Instruments). Absorption spectra were collected by using a PerkinElmer Lambda 750S UV-visible-NIR spectrometer. NIR-II fluorescence spectra were recorded on Edinburgh Fluorescence Spectrometer FLS980 instrument with external 808, 860 or 980-nm semiconductor laser (Changchun New Industries Optoelec-tronics Tech. Co., Ltd.) as excitation source. The NIR-II fluorescence *in vivo* imaging were performed with InGaAs array detector (Princeton Instruments, NIR vana 640).

General imaging setup

The imaging setup uses 808/860/980-nm lasers with same power density (depend on the requirements of each experiment) coupled into a 900-μm core metal-cladded multimode fiber (Changchun New Industries Optoelec-tronics Tech.). Fluorescence signal is directed from the imaging stage to the InGaAs SWIR camera (NIRvana 640; Princeton Instruments) using a combination of two long-pass emission filters (850 nm and 1000 nm long-pass; Edmund Optics) incorporated before camera lens. For each wavelength channel different filter sets were used to ensure no interference

between different wavelength signals (1100 nm short-pass for 1064 nm channel; 1200 nm long-pass for 1344 nm channel; 1200 nm and 1400 nm long-pass for 1550 nm channel). The InGaAs camera (NIRvana 640; Princeton Instruments) was cooled to −80 °C, the analog to digital (AD) conversion rate was set to 2 or 10 MHz, the gain was set to high, and different exposure times were used to achieve sufficient signal. All images were background and blemish corrected within the LightField imaging software and processed with Matlab.

Tissue phantom imaging study

1% Intralipid® made by volumetric dilution of a commercial 20% stock solution was chosen as a mock tissue because of its similar scattering properties.[3, 4] Glass capillary tube filled with cyclohexane solution of nanocrystal ($NaY_{0.95}Nd_{0.05}F_4$@$NaYF_4$ or $NaY_{0.5}Er_{0.5}F_4$@$NaYF_4$) was wrapped in black tape to leave 2 cm length available for imaging. The capillaries were then placed under a cylindrical dish and covered with different volumes of 1% Intralipid®. The depth of the capillary was calculated from the known area of the dish. Excitation was provided by 808-nm, 860-nm or 980-nm diode laser (Changchun New Industries Optoelec-tronics Tech. Co., Ltd.) coupled to a 900-μm core metal-cladded multimode fiber. Filter sets were used as mentioned above. Exposure times were extending for each image acquired at deeper penetration depth to ensure best signal-to-noise ratio. To obtain penetration depth information, average intensity was taken from the same ROI at various depths and corrected with corresponding exposure times. To determine feature width, linear cross-sections were taken from the images and fit to Gaussians using Origin's built-in curve fitting. Ratiometric images were processed with matlab software. Similar methods were used to obtain information from images.

NIR-II ratiometric imaging of lymphatic inflammation

Animal experiments were in agreement with the guidelines of Fudan University's Administrative panel on Laboratory Animal Care. Eight weeks old female mice were purchased from Shanghai SLAC Laboratory animal CO. Ltd. And the animal experiments were permitted by the Shanghai Science and Technology Committee. To establish the lymphmatic inflammation, mice were intradermally (i.d.) injected with 50 μL (2.5 mg/mL) lipopolysaccharide into the dorsal skin of the rear paw, and followed 4 h later by an additional i.d. injection of 100 μL DCNP@Cy7.5 (~0.35 mg for nanocrystal and 5 nmol Cy7.5), and thereafter imaged by a homebuilt NIR-II fluorescence imaging system. Before imaging, the mice were anaesthetized using rodent ventilator with 2 L min^{-1} air mixed with 4% isoflurane. Images at each channel (808-nm and 980-nm excitation, power density on the surface of mice was set to 80~125 mw/cm^2, exposure time was

set to 200 ms) were recorded at 0, 5, 10, 20, 30 min post-injection to visualize the dynamic drainage and finaly processed with matlab to get ratiometric images. All groups within study contained n = 3 mice.

Statistical analysis

All data were expressed in this manuscript and supporting information as mean ± s.d. All the results have been performed at least three times by independent experiments. No samples and animals were excluded from the analysis. A two-tailed Student's t test was used to analyse the statistical significance between two groups. The statistical analysis was performed by using OriginPro 2017 (Originlab Software Inc.). Asterisks indicate significant differences (*$P < 0.05$, **$P < 0.01$).

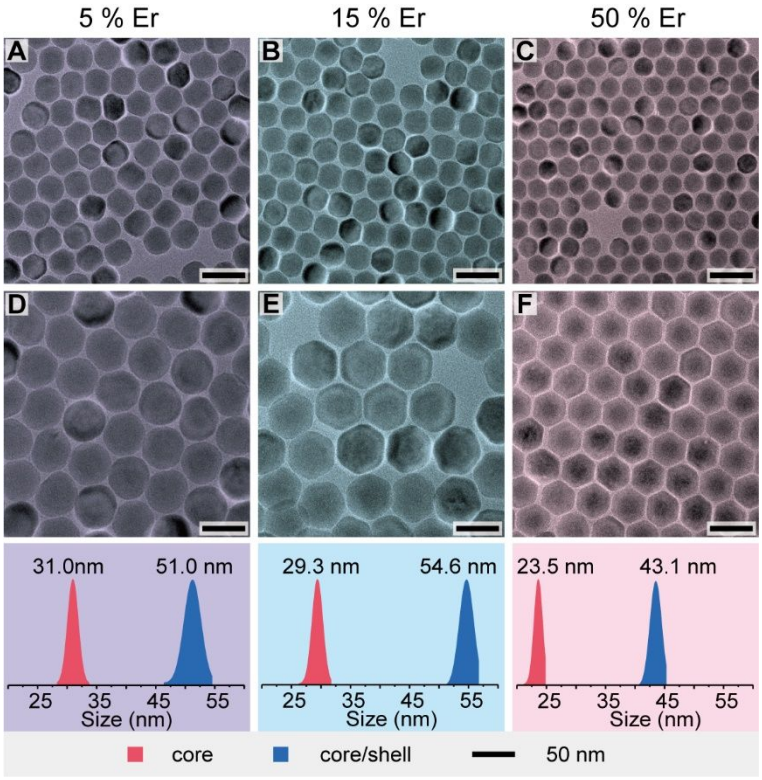

Figure S1. TEM images (upper) and the corresponding size distributions (lower) of the obtained nanocrystals. (A) $NaY_{0.95}Er_{0.05}F_4$ core and (D) $NaY_{0.95}Er_{0.05}F_4$@$NaYF_4$ core-shell nanocrystals. (B) $NaY_{0.85}Er_{0.15}F_4$ core and (E) $NaY_{0.85}Er_{0.15}F_4$@$NaYF_4$ core-shell nanocrystals. (C) $NaY_{0.5}Er_{0.5}F_4$ core and (F) $NaY_{0.5}Er_{0.5}F_4$@$NaYF_4$ core-shell nanocrystals.

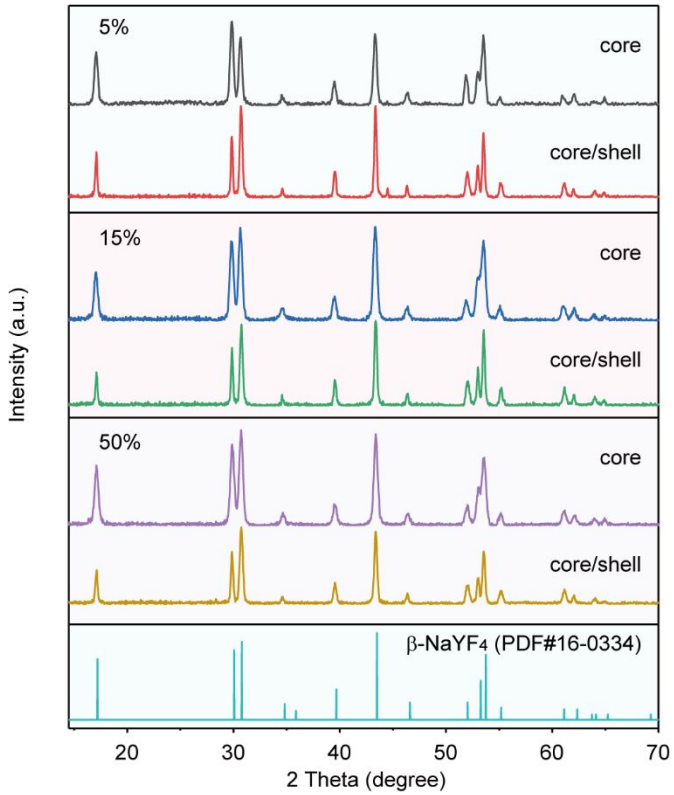

Figure S2. XRD patterns of the $NaY_{1-x}Er_xF_4$ core only and $NaY_xEr_{1-x}F_4$@$NaYF_4$ core/shell nanoparticles with different Er^{3+}-doping concentration (x = 0.05, 0.15 and 0.5), respectively.

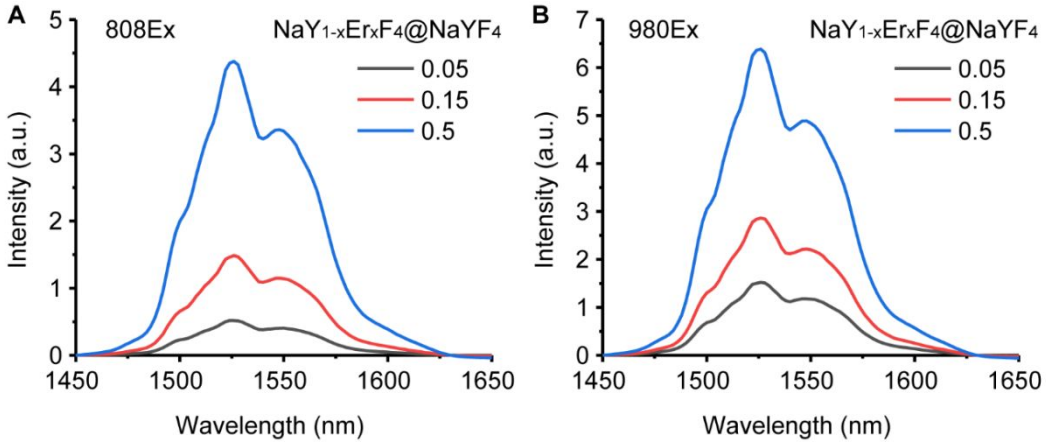

Figure S3. Fluorescence spectra of $NaY_{1-x}Er_xF_4$@$NaYF_4$ core/shell nanoparticles in cyclohexane with different Er^{3+}-doping concentrations (x = 0.05, 0.15 and 0.5) under 808-nm (A) and 980-nm (B) excitation, respectively.

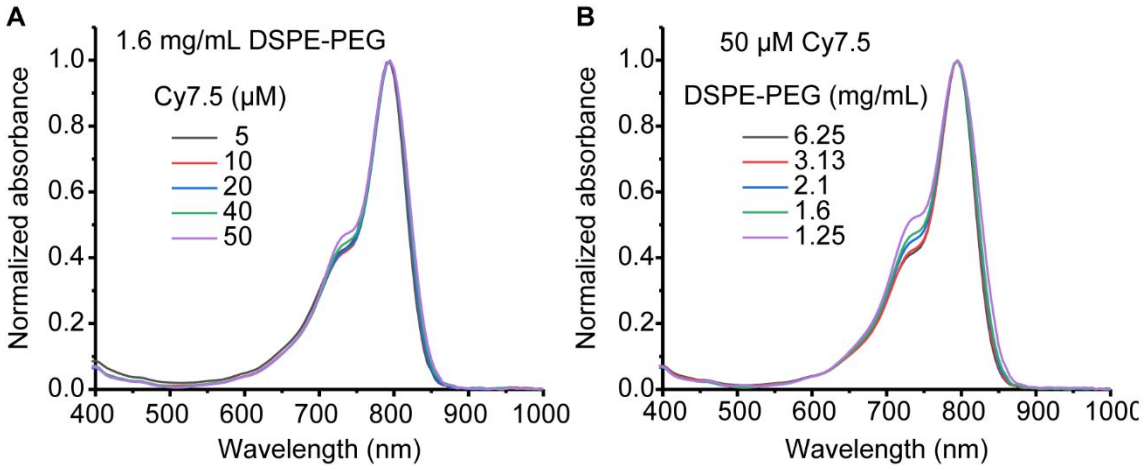

Figure S4 Normalized absorbance spectra of Cy7.5@DBCO nanomicelles (A) by varying Cy7.5 concentration with a fixed DSPE-PEG concentration, (B) by varying DSPE-PEG concentration with a fixed Cy7.5 concentration. The results show that a dye loading capacity of ~2 wt% (1.6 mg/mL DSPE-PEG and 50 μM Cy7.5) is appropriate without any broadening and reducing in absorption spectra.

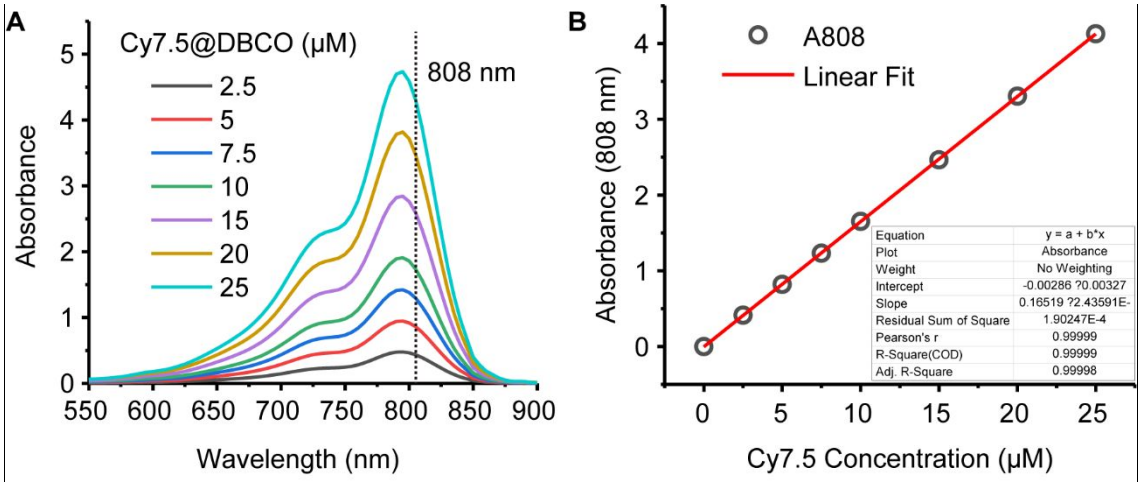

Figure S5 (A) Absorbance spectra of Cy7.5@DBCO with varying concentrations of Cy7.5. (B) Linear relationship of absorbance at 808 nm to Cy7.5 (0-25 μM).

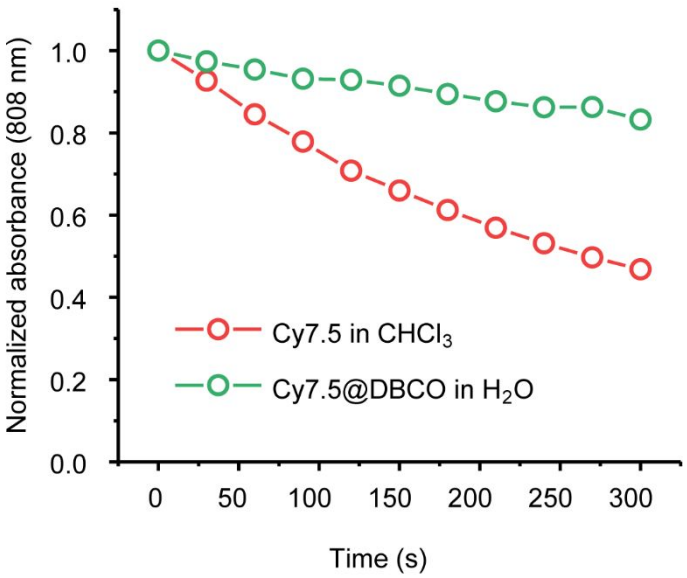

Figure S6. Photostability of Cy7.5 in $CHCl_3$ and Cy7.5@DBCO in H_2O under continuous 808-nm exposure for 5 min at a power density of 3.5 W/cm^2. The results verified the superior photostability of DSPE-PEG nanomicelles encapsulated Cy7.5, ensuring the accurate measurements of ratiometric signals. Note that the power density of 808-nm laser for spectra analysis and ratiometric imaging was much lower than 3.5 W/cm^2 and exposure times were controlled within 30 s for each test.

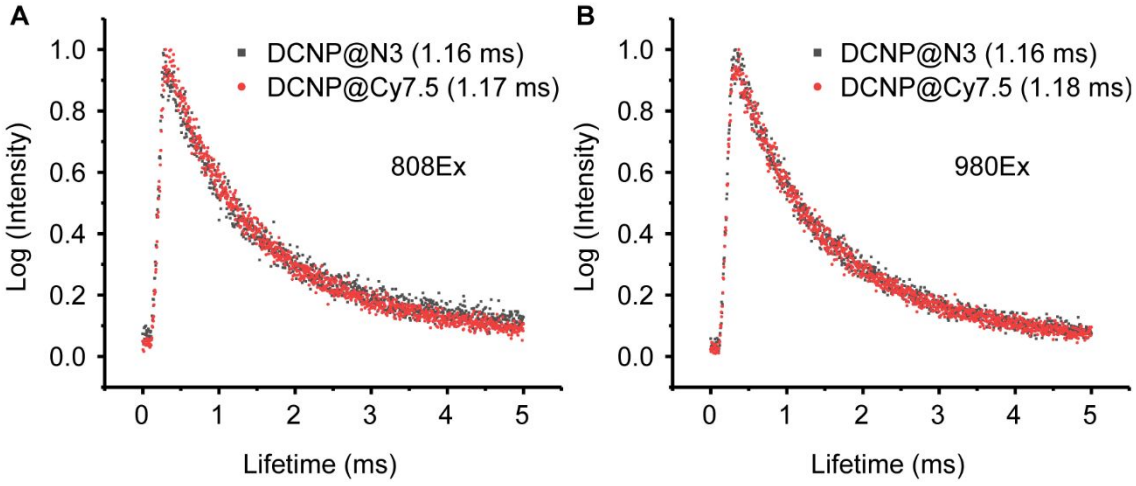

Figure S7. Fluorescence lifetime spectra of DCNP@N_3 and DCNP@Cy7.5 at 1550 nm emission under 808-nm (A) and 980-nm (B) excitation.

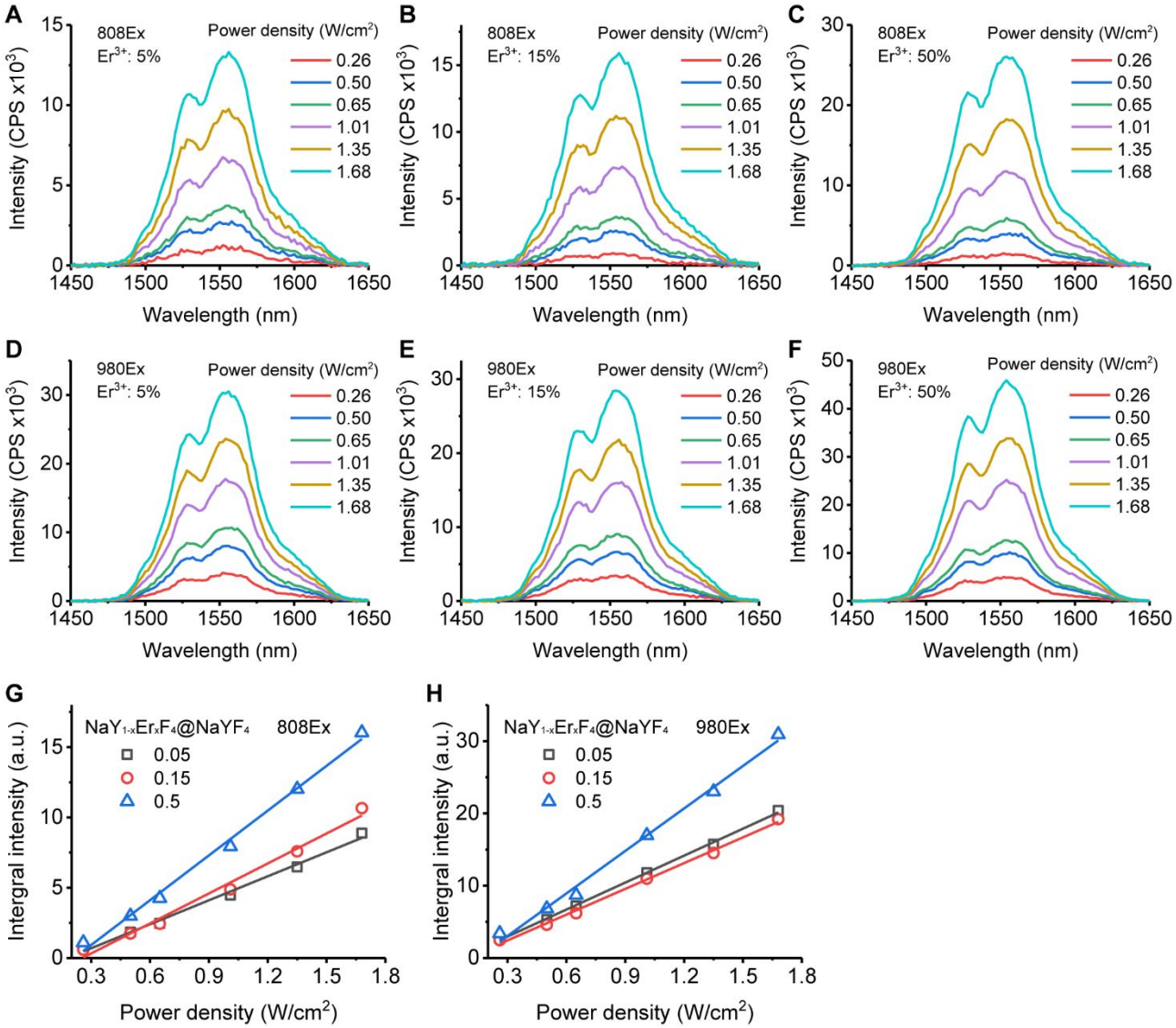

Figure S8. Power density dependence of fluorescence spectra of DCNP@N_3 nanoparticles with different Er^{3+} doping concentration under 808-nm and 980-nm excitation, respectively. (A, D) $NaY_{0.95}Er_{0.05}F_4$@$NaYF_4$, (B, E) $NaY_{0.85}Er_{0.15}F_4$@$NaYF_4$, (C, F) $NaY_{0.5}Er_{0.5}F_4$@$NaYF_4$. Linear power density dependence of fuorescence intensity at 1550 nm of DCNP@N_3 under 808-nm (G) and 980-nm (H) excitation, showing DCNP with 50 mol% Er^{3+} has the most sensitive power dependent fluorescence property.

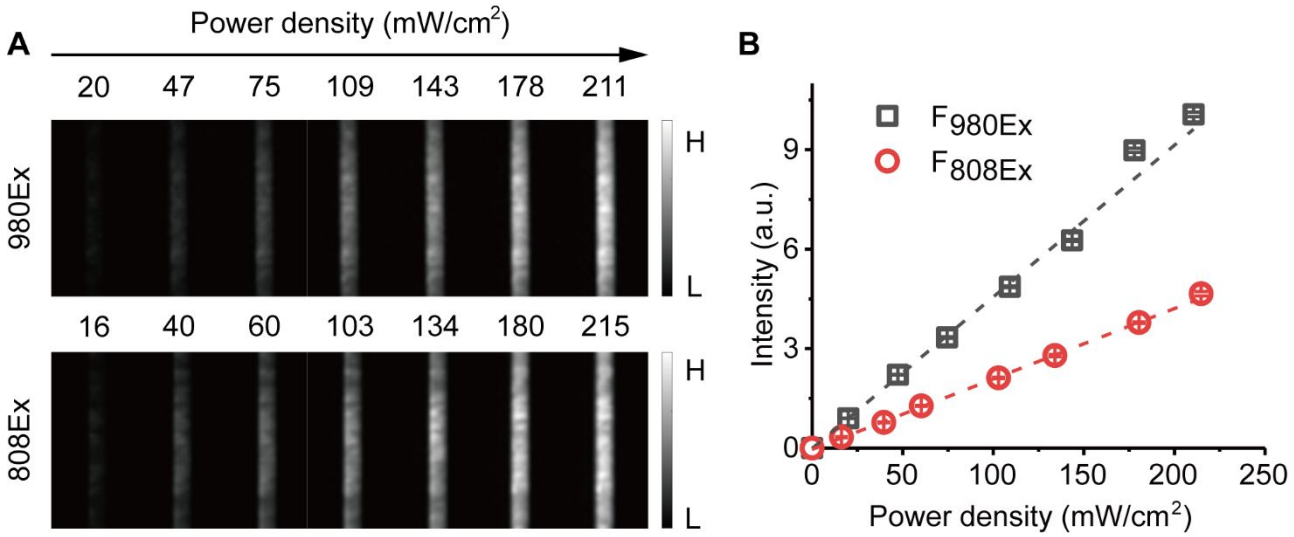

Figure S9. (A) NIR-II fluorescence images of capillary tube filled with DCNP@N_3 under 808-nm and 980-nm excitation with varying power density. (B) Linear relationship of fluorescence intensity acquired from the images with the excited power density. The results illustate that the fluorescence intensity of DCNP@N_3 show linear relationship with excited power density of *in vivo* imaging.

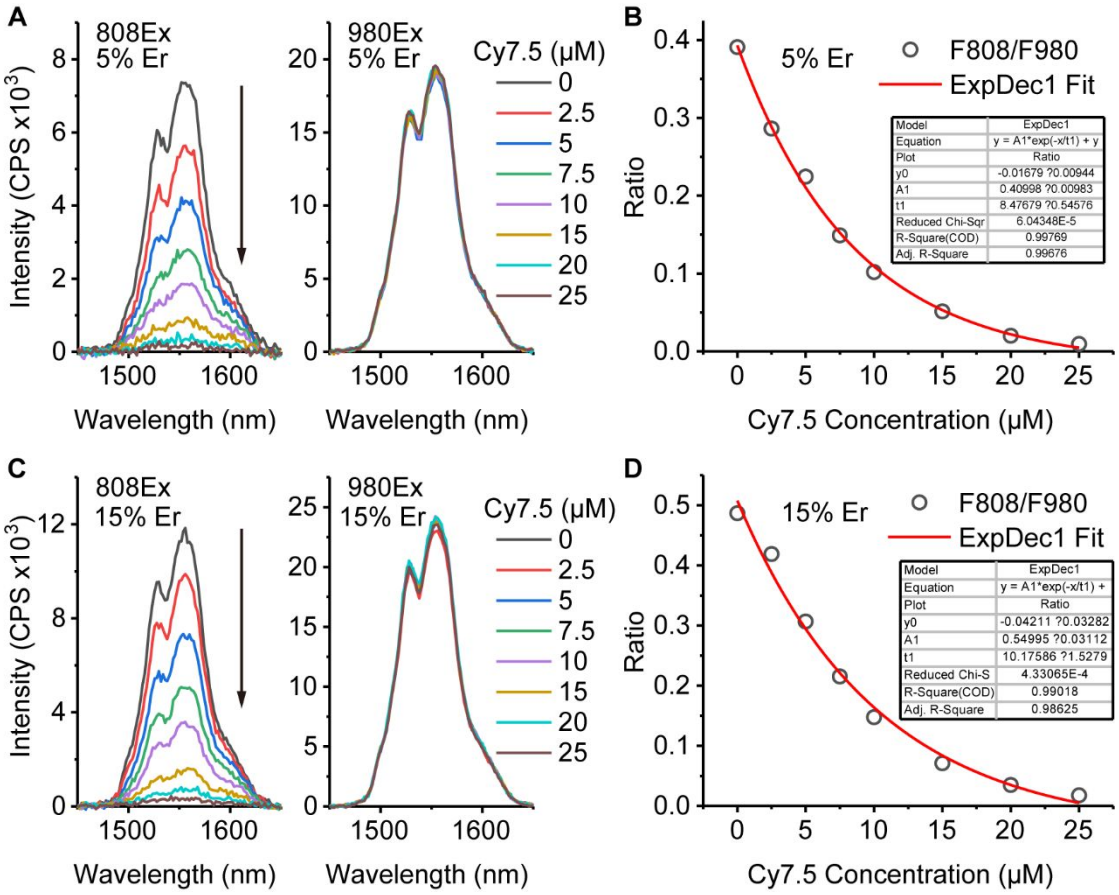

Figure S10. Fluorescence spectra of $NaY_{0.95}Er_{0.05}F_4$@$NaYF_4$ (A) and $NaY_{0.85}Er_{0.15}F_4$@$NaYF_4$ (C) with varied concentrations of Cy7.5 (0-25 μM) under 808-nm and 980-nm excitation respectively. Plot of fluorescence ratio changes of $NaY_{0.95}Er_{0.05}F_4$@$NaYF_4$ (B) and $NaY_{0.85}Er_{0.15}F_4$@$NaYF_4$ (D) as a function of Cy7.5 concentration, which could be well fitted by single exponential function.

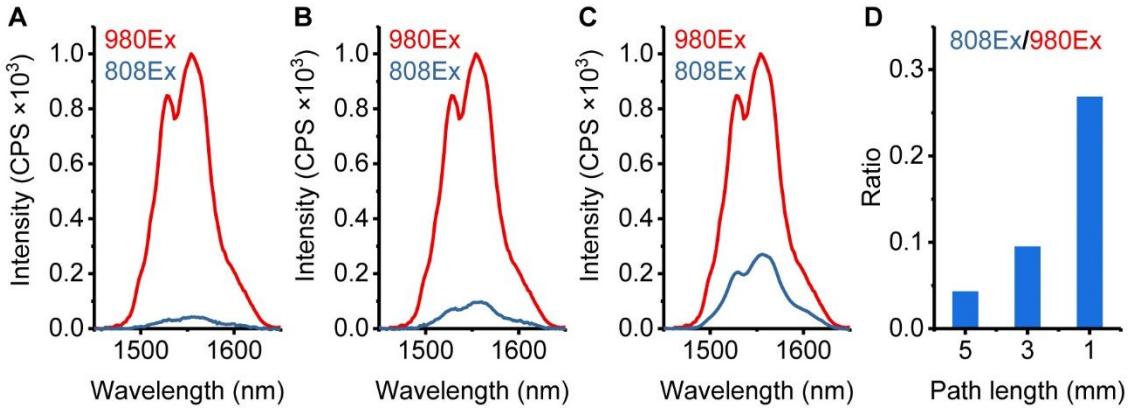

Figure S11. (A-C) Normalized fluorescence spectra of DCNP with fixed concentrations of Cy7.5 (15 μM) under 808-nm and 980-nm excitation respectively. The path lengths of excitation light were set to 5 mm (A), 3 mm (B), 1 mm (C). (D) Fluorescence ratio ($F_{1550Em,\ 808Ex}/F_{1550Em,\ 980Ex}$) of DCNP with varied optical path lengths. DCNP: $NaY_{0.5}Er_{0.5}F_4$@$NaYF_4$, ~2.4 mg/mL containing ~0.26 mg/mL of Er^{3+}. The results demonstrate the similar effect of optical path length and concentration of absorber on the ACIE mechanism.

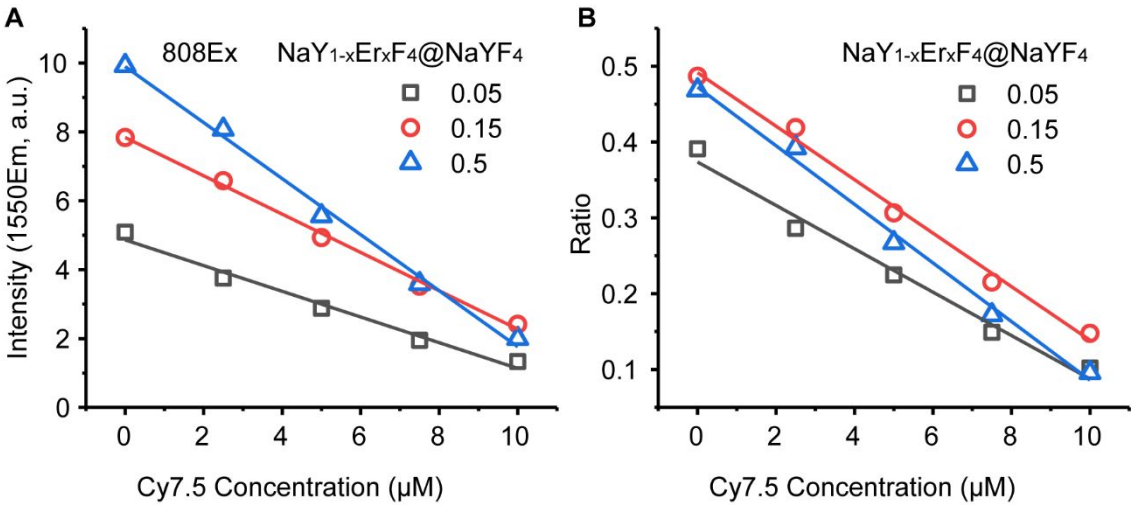

Figure S12. (A) Comparison of fluorescence intensity at 1550 nm of $NaY_{1-x}Er_xF_4$@$NaYF_4$ (x = 0.05, 0.15 and 0.5) under 808-nm excitation with varying concentration of Cy7.5 (0-10 μM). (B) Comparison of fluorescence ratio (F(1550Em, 808Ex)/F(1550Em, 980Ex)) of $NaY_{1-x}Er_xF_4$@$NaYF_4$ (x = 0.05, 0.15 and 0.5) with varied concentration of Cy7.5 (0-10 μM). Linear fitting for both fluorescence intensity and ratio data shows the most sensitive response occurred at Er^{3+}-doped concentration of 50 mol%.

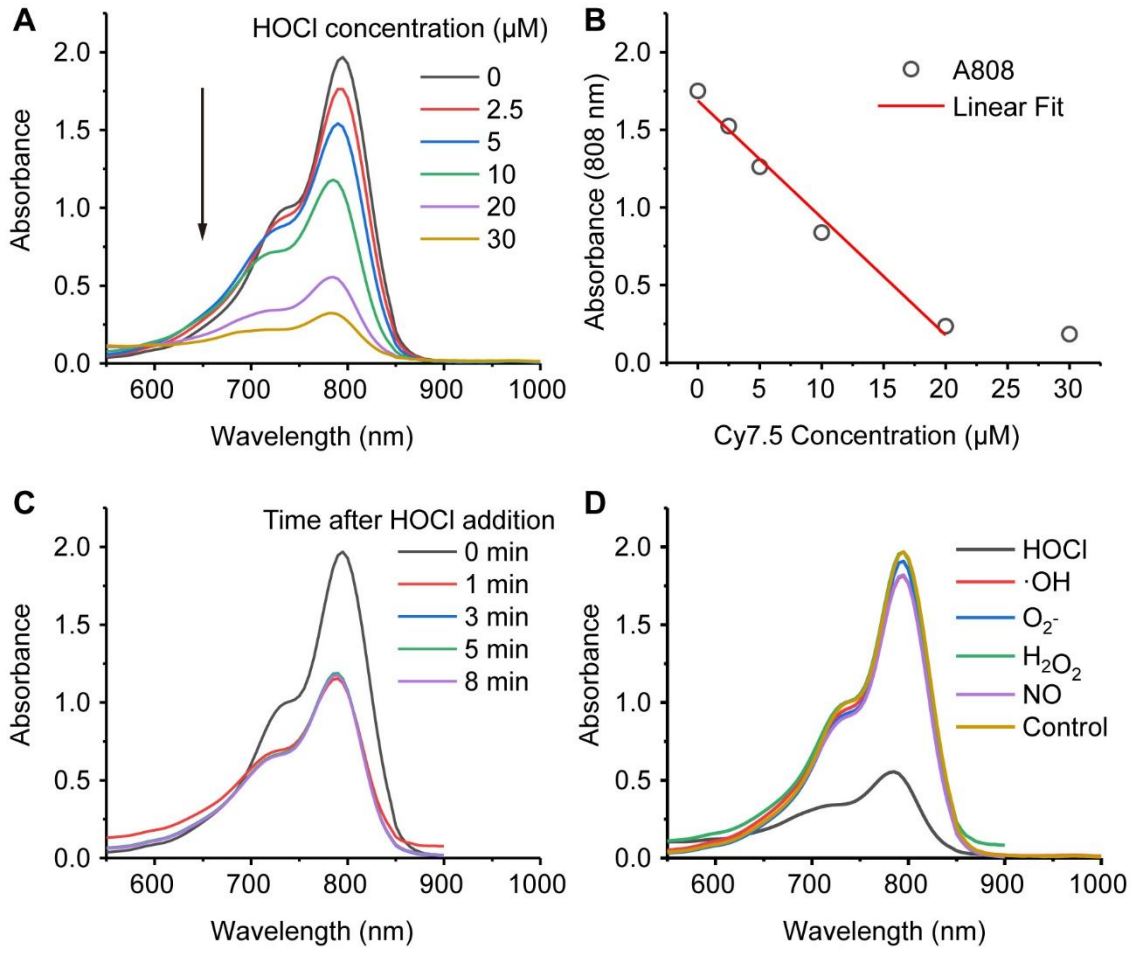

Figure S13. (A) Absorbance spectra of Cy7.5@DBCO (10 μM) in aqueous solution upon addition of 0-30 μM HOCl. (B) Plot of absorbance at 808 nm as a function of HOCl concentration. (C) Time dependent absorbance spectra of Cy7.5@DBCO (10 μM) in aqueous solution upon addition of 10 μM HOCl showing the response time is less than 1 min. (D) Absorbance spectra of Cy7.5@DBCO (10 μM) in aqueous solution toward various ROS (100 μM for H_2O_2, $O_2^{\bullet-}$, NO, 50 μM $^{\bullet}$OH and 20 μM HOCl).

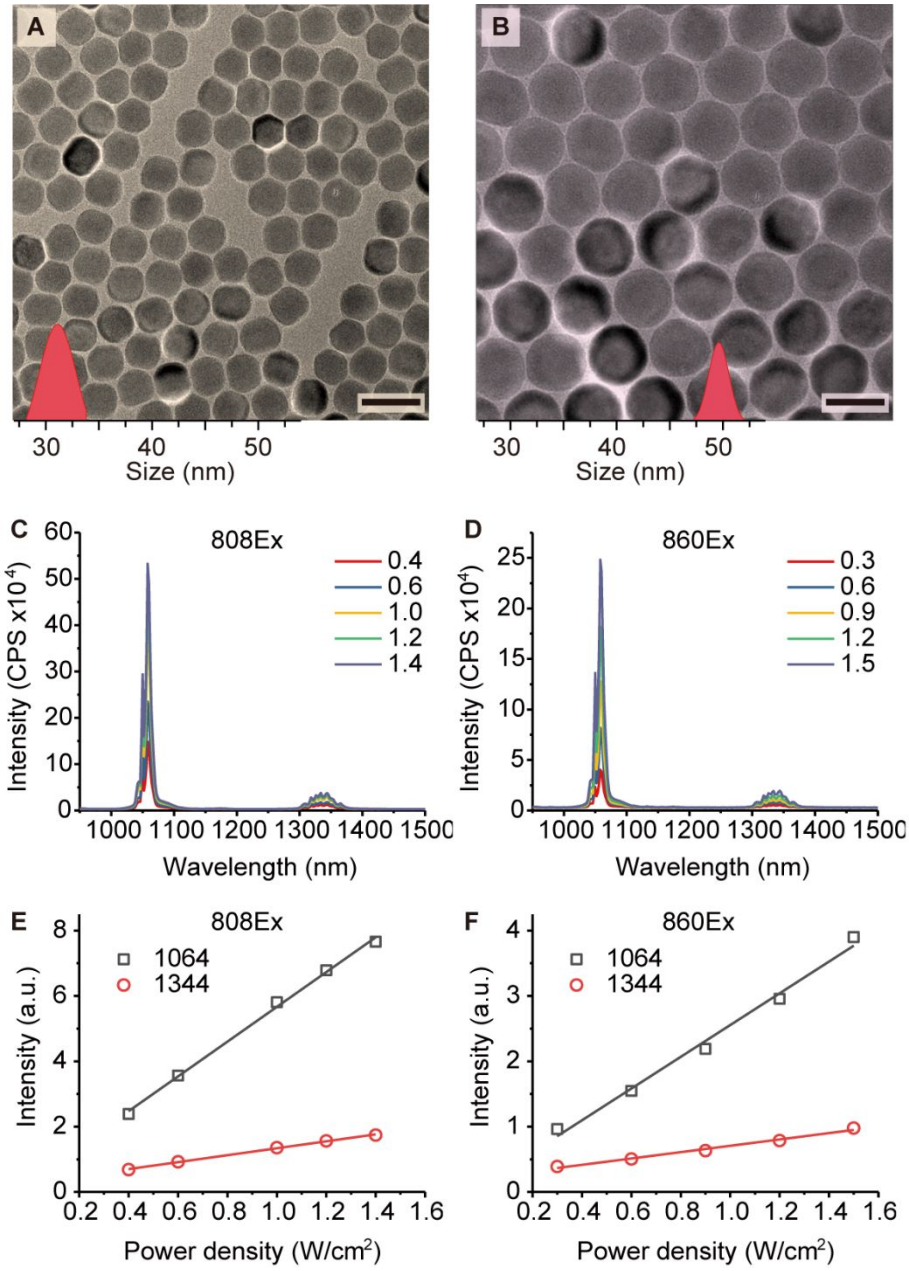

Figure S14. TEM images and the corresponding size distributions of $NaY_{0.95}Nd_{0.05}F_4$ core (A) and $NaY_{0.95}Nd_{0.05}F_4$@$NaYF_4$ core/shell (B). (C) Power density dependence of fluorescence spectra of $NaY_{0.95}Nd_{0.05}F_4$@$NaYF_4$ in cyclohexane under 808-nm (C) and 860-nm (D) excitation, respectively. Linear power density dependence of fluorescence intensity at 1064 nm and 1344 nm under 808-nm (E) and 860-nm (F) excitation, respectively.

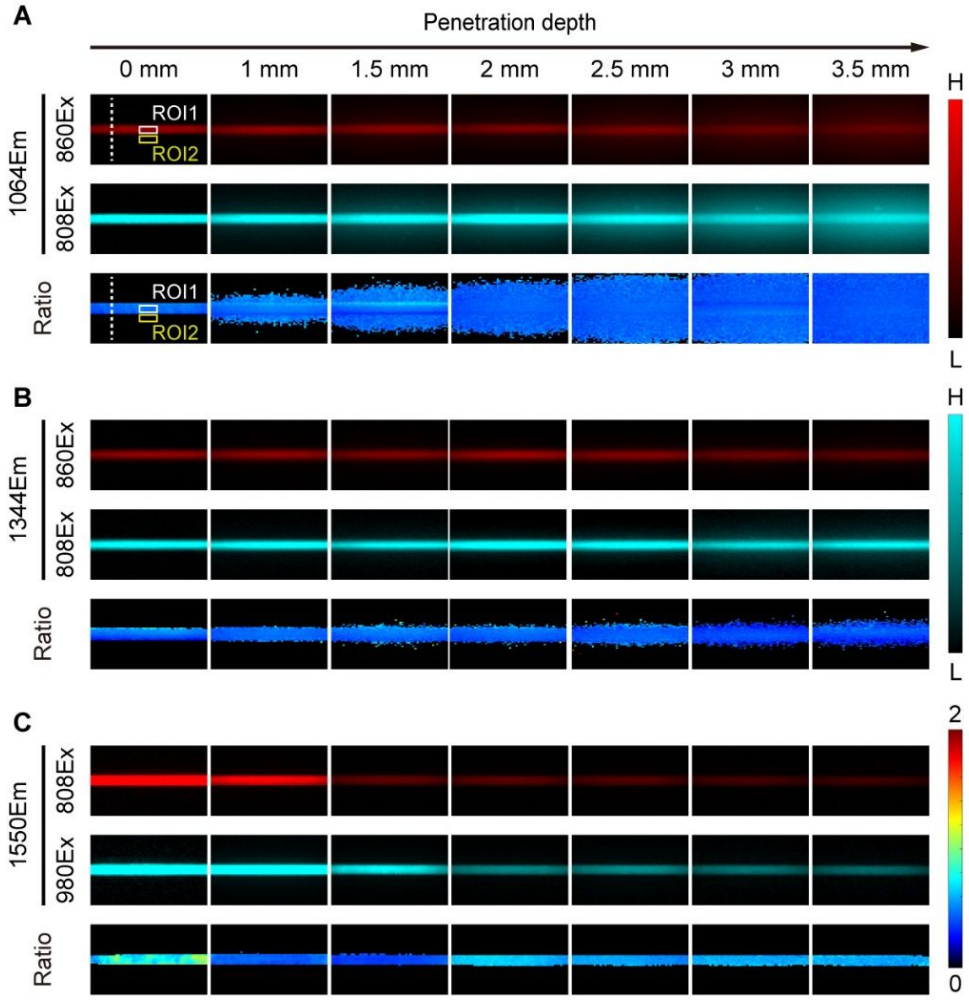

Figure S15. NIR-II fluorescence images (1064Em, 1344Em and 1550Em) and corresponding ratiometric images (Ratio) of capillary immersed in 1% Intralipid with varied depth of 0 mm-3.5 mm. 1064Em and 1344Em are collected from Nd^{3+}-doped DCNP under 808-nm and 860-nm excitation. 1550Em is collected from Er^{3+}-doped DCNP under 808-nm and 980-nm excitation.

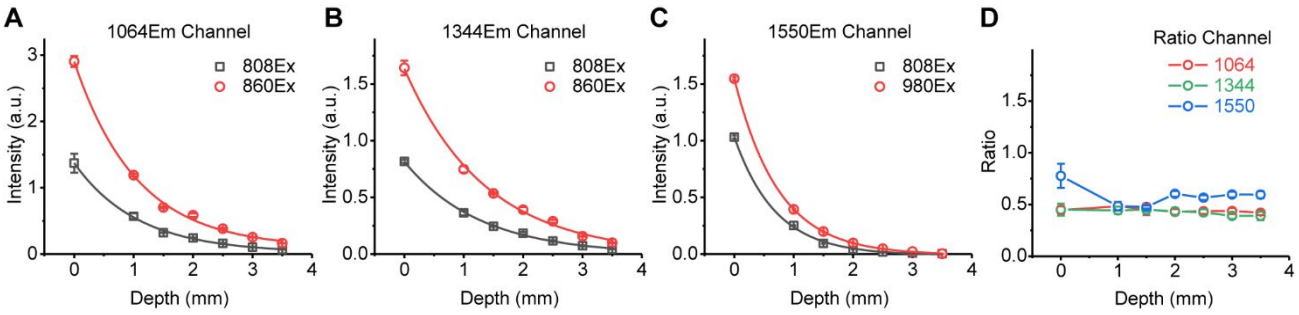

Figure S16. Intensity decay of 1064 nm (A) and 1344 nm (B) emission (808-nm and 860-nm excited) from $NaY_{0.95}Nd_{0.05}F_4$@$NaYF_4$, and 1550 nm (C) emission (808-nm and 980-nm excited) from DCNP@N_3 as a function of depth in 1% Intralipid, respectively. (D) Ratiometric signals of 1064, 1344 and 1550 ratio channel in Figure 3C as a function of depth in 1% Intralipid. Within the depth range of 1-3.5 mm, the ACIE ratiometric signals are relative reliable with low coefficient of variations (< 11% for 1550 ratio channel, < 6% for both 1064 and 1344 nm ratio channels).

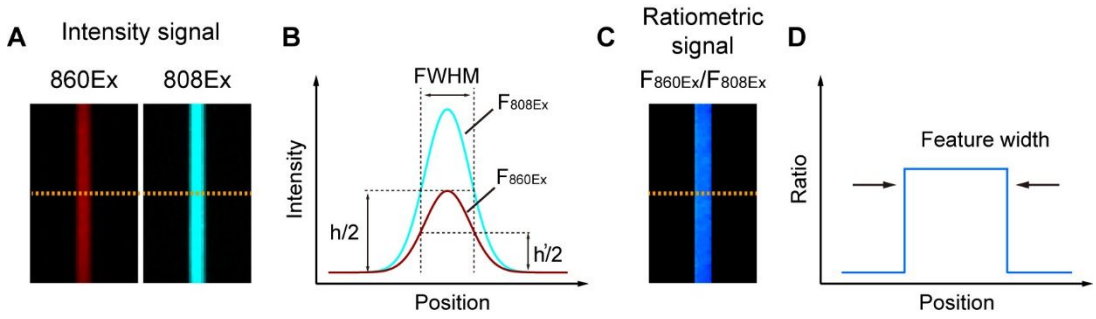

Scheme S3. Schematic illustration showing the "leveling effect" of signal in raitometric channel after internal normalization. (A, B) Representative fluorescent images (A) and corresponding ratiometric image (B) of a capillary tube filled with sample. (B, D) Representative cross-sectional intensity profiles (B) and corresponding ratio profile (D) along the orange-dashed bars in A and C, respectively.

Supplementary note 1. The leveling effect of ratiometric fluorescence imaging.

For a given emission wavelength, cross-sectional intensity profiles of capillary excited by different wavelengths follow the same Gaussian distribution, which are independent to signal strength. This means, ideally, the ratio between two fluorescent signals derived from a division operation (F_{860Ex}/F_{808Ex}) is a constant, thus showing a "square wave"-like distribution along the cross-sectional line. In other words, the difference between the center signal and the edge signal in intensity profiles is leveled in ratio channel. Therefore, when there is a scattering background around the capillary tube, although the true capillary signal can be resolved from fluorescent imaging, it will lose contrast to the background in ratio channel. This phenomenon is similar to the "leveling effect" in chemistry. If we define the full width at half maximum (FWHM) of Gaussian distribution in B as resolution of fluorescent signals, and feature width in D as the resolution of ratiometric signal, thus when the feature width of ratiometric signal is ideally 2-fold broader than the FWHM of fluorescent signal, ratiometric imaging should have the same resolution as fluorescent imaging.

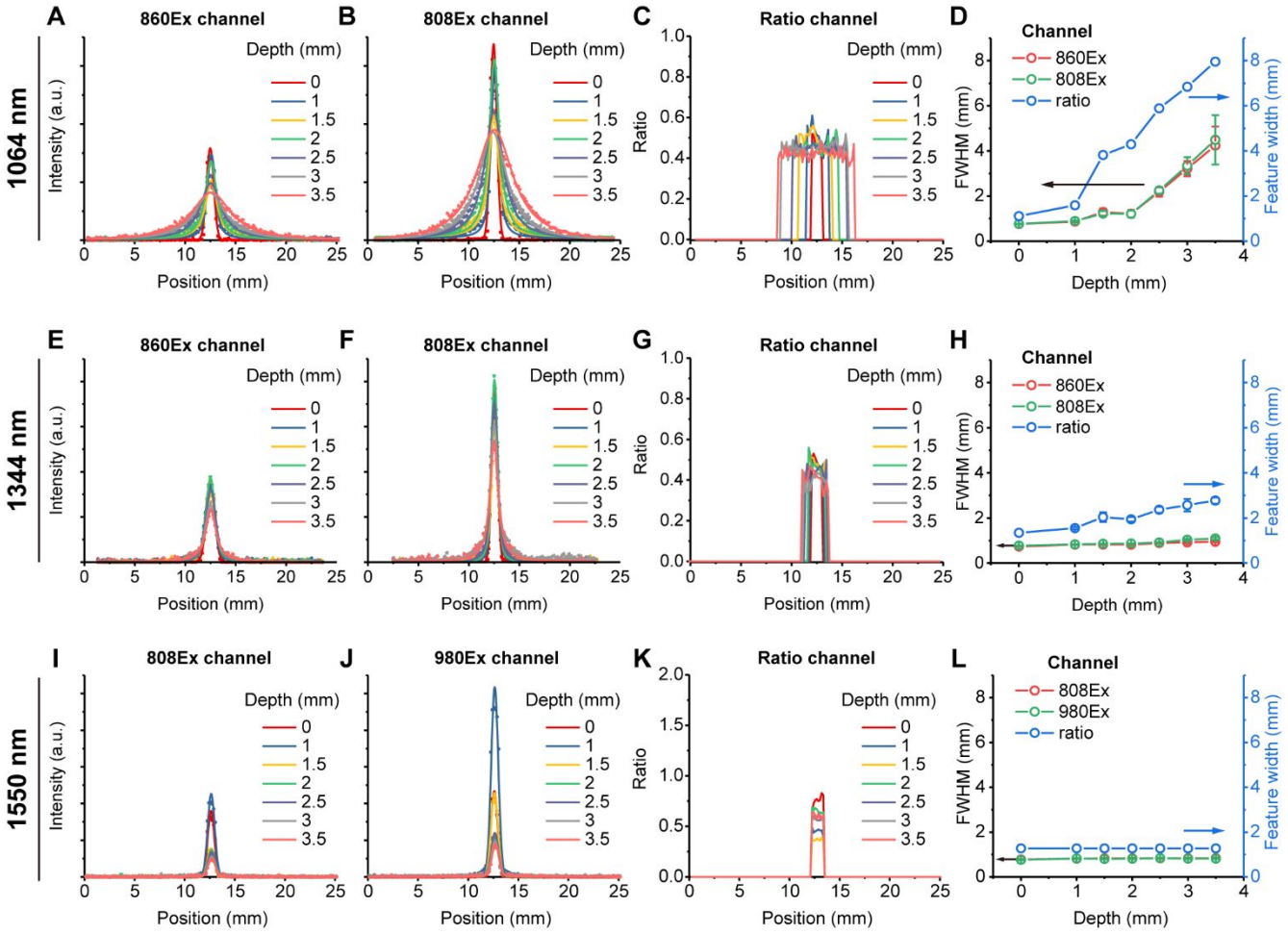

Figure S17. Cross-sectional fluorescence intensity (A, B, E, F, I, J) and ratio (C, G, K) profiles of capillary tubes images in Figure 3C. (A, B) 1064Em channel, (E, F) 1344Em channel, (I, J) 1550Em channel, (C) 1064 ratio channel, (G) 1344 ratio channel, (K) 1550 ratio channel. (D, H, L) FWHM (fluorescence signals) and Feature width (ratiometric signals) of capillary tubes as a function of depth. The results show feature width of capillary tubes in ratiometric images are all approximate 2-fold larger than FWHM of capillary tubes in fluorescent images as explained in **Scheme S3**.

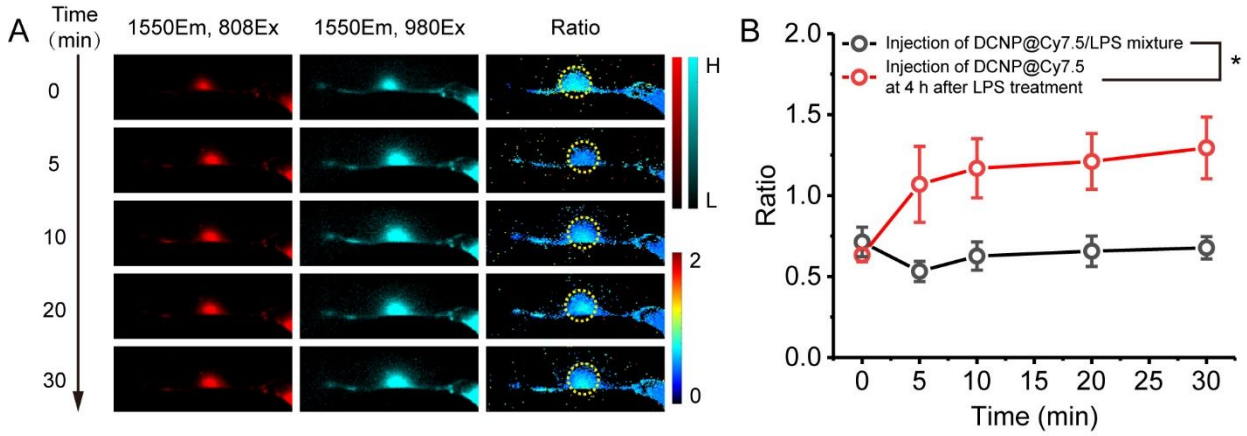

Figure S18. (A) *In vivo* NIR-II fluorescence imaging and ratiometric fluorescence imaging of lymphatic drainage in normal mice at different time points after injection of DCNP@Cy7.5/LPS mixture. (B) Ratiometric signals of popliteal lymph node (white dotted circle) in A over time, in comparison with that of LPS-treated group in **Figure 5E**. The bars represent mean ± s.d. derived from n = 3 biologically independent mice. *p* values were analyzed between LPS-treated mice and normal mice at all time points starting from 5 min by Student's two-sided t-test (*$P < 0.05$). The results show that simply mixing the NIR-II ratiometric nanoprobe with LPS alone did not lead to ratiometric signal changes over time.

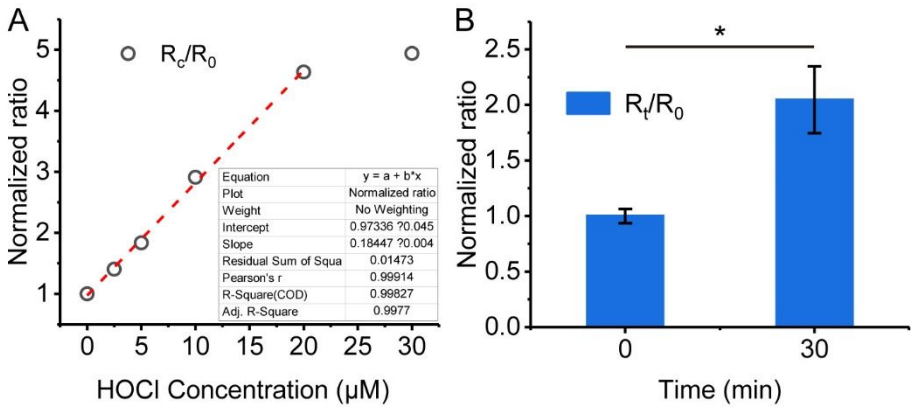

Figure S19. (A) Normalized ratio values versus HOCl concentration in vitro, corresponding to Figure 2F. (B) Normalized ratio changes versus time in LPS-treated group. All ratios at different concentrations of HOCl (R_c) or during different times of inflammatory response (R_t) were normalized by the original ratio value (R_0).

Supplementary note 2. Quantification of HOCl in inflammation site.

The optical signal calibration curve *in vitro* isn't suitable for *in vivo* quantification due to the obvious signal attenuation in biological tissue. But if we could take the signal fluctuation coefficient in mimic tissue into account, an estimated concentration of HOCl may be derived. In this work, the ACIE nanoprobes show signal fluctuation varying with penetration depth due to the dual-excitation wavelength (808/980 nm). The coefficient of variation of ratiometric signals is about 10.5% (Figure S16). Thus, according to the following calculations, the estimated concentration of HOCl is 7.0±2.0 μM during 30 minutes of inflammatory response.

By linear fitting of the plot in Figure S19, the calibration function is given by

$$R_c = 0.97336 + 0.18447c$$

where c is the concentration of HOCl, R_c is the ratio at the HOCl concentration of c (μM). The normalized ratio signal during 30 minutes of inflammatory response is about 2.05±0.34. By multiplying the fluctuation coefficient ($R_c = R_t \times 1.105$), the corrected ratio is about 2.26±0.37. Therefore, we can derive the concentration of HOCl to be ~7.0±2.0 μM during 30 minutes of inflammatory response by means of the calibration function.

References

[1] F. Wang, R. Deng, X. G. Liu, *Nat Protoc.* **2014**, *9*, 1634.

[2] X. Li, D. Shen. J. Yang, C. Yao, R. Che, F. Zhang, D. Zhao, *Chem. Mater.* **2013**, *25*, 106.

[3] H. J. van Staveren, C. J. M. Moes, J. van Marie, S. A. Prahl, M. J. C. van Gemert, *Appl. Opt.* **1991**, 30, 4507.

[4] F. S. T., J. S. L., W. B. C., S. W. M., v. G. M. J. C., *Lasers Surg. Med.* **1992**, 12, 510.